SPACE TELESCOPE SCIENCE INSTITUTE
Operated for NASA by AURA

Instrument Science Report STIS 2006-02

Spectroscopic PSF: Comparison of Data and Models for a Target Centered In and Out of the Aperture

Linda Dressel
April 10, 2006

ABSTRACT

Long-slit spectroscopic observations of a star, using the G750L grating with perpendicular-to-slit stepping patterns, are compared with models based on the Tiny Tim STIS imaging PSF. When the star is centered in the aperture (52x0.1, 52x0.1E1, 52x0.2, or 52x0.2E1), the observed flux exceeds the model predictions at distances greater than 0.2 arcsec from the center of the star, at flux levels below a few percent of the peak, due to scattering and diffraction. When the star is moved out of the aperture by one or two slit widths, the flux is less than predicted from the modelling. Possible reasons for this discrepancy are examined. The G750L grating and the mirror used for CCD imaging each have a Lyot stop in their optical path, which broadens the PSF and requires an empirical adjustment in the modelling of narrow-slit spectroscopic PSFs. The G750M grating, often used for spatially resolved spectroscopy, does not have a Lyot stop. The effect of the Lyot stop on the PSF is shown in a comparison of the PSFs (observed and modelled) for target-centered pointings using the G750M and G750L gratings.

Introduction

Many observing programs have used STIS to map sources spectroscopically. Typically, one of the narrow slits is stepped by its width a few times to cover the region of interest. The finite point spread funcion (PSF) spreads flux from row to row in a spectroscopic image, and across the slit from sources located in and out of the slit. This contaminating flux must be accounted for in modelling the velocity structure and surface

brightness structure of the region. For example, measurements of black hole mass are being made by applying instrumental effects to models of nuclear gaseous disks to produce emission line profiles for comparison to observed line profiles. One step in this procedure is to convolve a model brightness distribution at a given wavelength with the point spread function at that wavelength. PSFs generated by the publically available Tiny Tim software are generally used, although they were developed for STIS imaging rather than spectroscopy. Since differences in the optics in the imaging and spectroscopic light paths produce differences in the PSF at the detector, beyond the dispersion introduced by the gratings, point source observations are used here to test the models for spectroscopic applications.

Observations and Data Reduction

Spectroscopic observations of HD73471, a bright K star (V = 4.45 mag), were obtained in STIS calibration program 9610 on 29 September 2002. The 52x0.1 slit was stepped in a perpendicular-to-slit pattern of five 0.1-arcsec steps centered on the star. Similary, the 52x0.2 slit was stepped in a perpendicular-to-slit pattern of three 0.2-arcsec steps centered on the star. Both patterns were repeated at the E1 aperture positions, which place the target near the readout end of the CCD detector to reduce CTI losses. The G750L grating was used at central wavelength setting 7751 to make data available for spectroscopic PSFs from 5240 to 10260 Å. For each slit position, four dither steps were performed along the slit at 3.5 pixel intervals to give half-pixel sampling and redundant pairs of observations (dithers of 0 and 7 pixels, 3.5 and 10.5 pixels). The exposures were short (0.8 sec for the 52x0.1 slit, 0.5 sec for the 52x0.2 slit), so the images could be used separately without cosmic ray rejection.

ACQ/PEAKs were used to obtain pointing with an accuracy of 0.005 arcsec. The observations were done in the sequence ACQ, 52x0.1 ACQ/PEAK, 52x0.1 pattern, 52x0.1E1 ACQ/PEAK, 52x0.1E1 pattern, 52x0.2E1 pattern, 52x0.1 ACQ/PEAK, 52x0.2 pattern. All but one of the twenty exposures in the 52x0.1 pattern were completed within one orbit (49 minutes). Three slit positons of the 52x0.1E1 pattern were executed within one orbit and the remaining two slit positions extended into a second orbit. The 52x0.2 and 52x0.2E1 patterns were each completed in a timespan of less than 20 minutes. The driftrate of HST is less than 0.01 arcsec per hour, and thermal drifts are generally less. Small angle pointing manuevers have errors less than 0.003 arcsec (STIS Instrument Handbook, Kim Quijano et al. 2003).

Data were taken from the standard flt images, which have been corrected with bias, dark, and flat reference files. A single column at 6600 Å in each spectral image was taken as the observational PSF. 6600 Å was chosen as representative of the H alpha region of the spectrum. Comparison of the redundant pairs of dithered observations showed that the flux errors were not dominated by the formal errors included in the error arrays, but rather by other errors such as slightly inaccurate dither steps. Averaging over columns would therefore not improve the accuracy of the results.

Modelling

Model HST imaging PSFs can be produced using Tiny Tim software (http://www.stsci.edu/software/tinytim/) provided by Krist and Hook. To generate a CCD spectroscopic PSF, the aperture is placed on a finely sampled monochromatic imaging PSF and the flux within the aperture is summed along the dispersion direction. The summed fluxes are blocked into pixels in the cross-dispersion direction, then a convolution is performed to simulate charge diffusion on the CCD. The imaging PSF appropriate to the grating should be used: generated with a Lyot stop in the optical path (default Tiny Tim parameters) or without a Lyot stop (customized Tiny Tim

parameters). This method of generating the spectroscopic PSF must be modified for the gratings that have a Lyot stop, to take into account the difference between the imaging PSF sampled at the aperture and the imaging PSF modelled on the detector. An empirical modification using a simple scaling of the PSF is described and tested below.

Lyot stops are mounted in front of the optical elements G430L, G750L, and MIRVIS (the mirror used for CCD imaging), close to the pupil plane (Chuck Bowers, private communication). These circular apertures are designed to supplement the focal plane mask used in coronographic mode by suppressing residual scattered and diffracted starlight from the collimated beam (Heap et al., 2000), but they do so at the expense of broadening the PSF. The stops are all nearly the same size (15.5 mm for MIRVIS and G430L, 15.0 mm for G750L; George Hartig, private communication), so this investigation will use the MIRVIS PSF to model the spectroscopic PSF for G750L. For first order CCD gratings other than G430L and G750L, the Lyot stop can effectively be removed from the Tiny Tim model by enlarging it to the point that the PSF becomes insensitive to its size.

The effect of the Lyot stop on the size of the PSF must be determined so that sampling of the PSF in the slit plane can be modelled appropriately. A comparison of the radial profile of light for model imaging PSFs at 6600 Å with and without the Lyot stop is shown in Figure 1. The PSFs were normalized to the same total flux. Each PSF, subsampled by 0.1 CCD pixel, was divided into quadrants centered on the X and Y axes. An annular average of flux as a function of distance from the center was computed for the two X quadrants taken together, and for the two Y quadrants taken together. The resulting X and Y flux profiles for the models with (solid lines) and without (dashed lines) the Lyot stop are shown in the upper panel of the figure. The Lyot stop model, which effectively sees a smaller diameter primary mirror, has a broader Airy disk and a slightly more distant first Airy ring. For each model, the X and Y profiles are very similar, showing the degree of X-Y symmetry of the models. In the lower panel of the figure, the model with no Lyot stop has been expanded radially by 10%, and the total flux has been conserved. The profiles for the expanded model are seen to be a good match to the profiles for the model with the Lyot stop. The implication of this comparison, that the Lyot stop broadens the PSF by 10% at 6600 Å, has been used in the application of spectroscopic apertures to the PSF for G750L. The slit has been broadened by 10% when applied to the Lyot-stopped imaging PSF, to compensate for the 10% narrower PSF in the aperture plane. The detailed features of the Lyot-stopped PSF are thus preserved, and the extent of the PSF in the cross-dispersion direction at the detector is maintained, but the sampling by the slit is improved.

If necessary, the input parameters for Tiny Tim can be adjusted for changes in focus. The spectroscopic PSF nominally has slightly better focus than the imaging PSF, but this was almost exactly compensated for by the average amount of defocus found to be in effect at the time of the observations for program 9610. (http://www.stsci.edu/hst/observatory/focus/ gives measurements of focus.) An additional consideration is the variation in focus that occurs during the course of an orbit due to thermal changes in the optical bench, a phenomenon referred to as breathing. A temperature-based model of breathing indicates that the excursion of the focus from the mean was up to +/-1.5 microns of secondary mirror motion during the observations, which should produce a negligible change in the PSF.

An image of the subsampled (0.1 pixel) 6600 Å Lyot-stopped PSF is shown in Figure 2, with overlays of the 5 placements of the (broadened) 52x0.1 slit and the 3 placements of the (broadened) 52x0.2 slit used in the observations. The trefoil structure in the first Airy ring is caused by the three support pads on the HST primary mirror. Profiles of the central 10 rows of the subsampled PSF image (spanning one CCD pixel along the slit) are shown in Figure 3. The locations of the edges of the slit are indicated in the figure. Near the central row of the PSF image, the first Airy ring is centered in the intermediate slit positions of the 52x0.1 observing pattern. It is at the edges of the 52x0.2 slit for all 3 positions of that observing pattern.

The subsampled PSF was summed over grids of 22 by 10 subpixels to represent (broadened) slitwidth

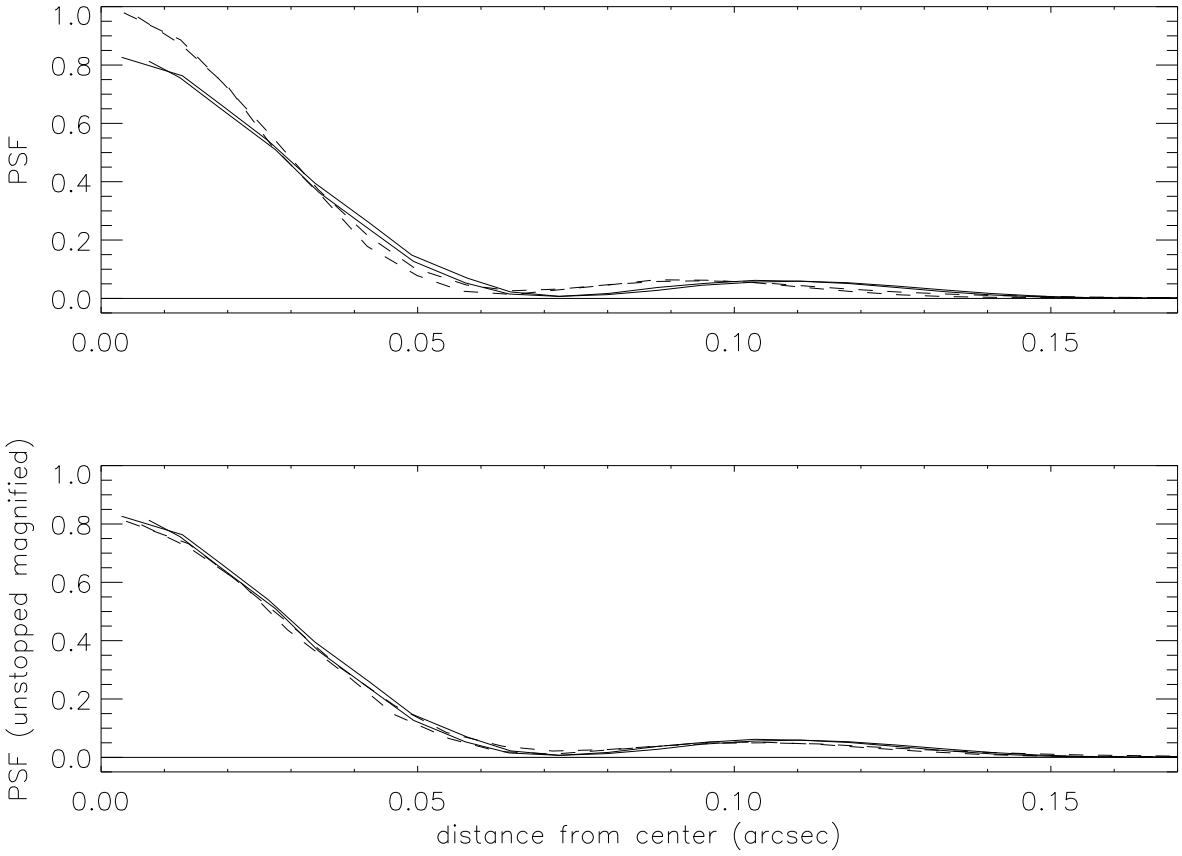

Figure 1: Upper panel: Profiles of annular averages of the X and Y quadrant fluxes for the Lyot-stopped PSF (solid lines) and unstopped PSF (dashed lines). Lower panel: Same as upper panel except that the unstopped PSF has been expanded by 10% in radius with conservation of flux.

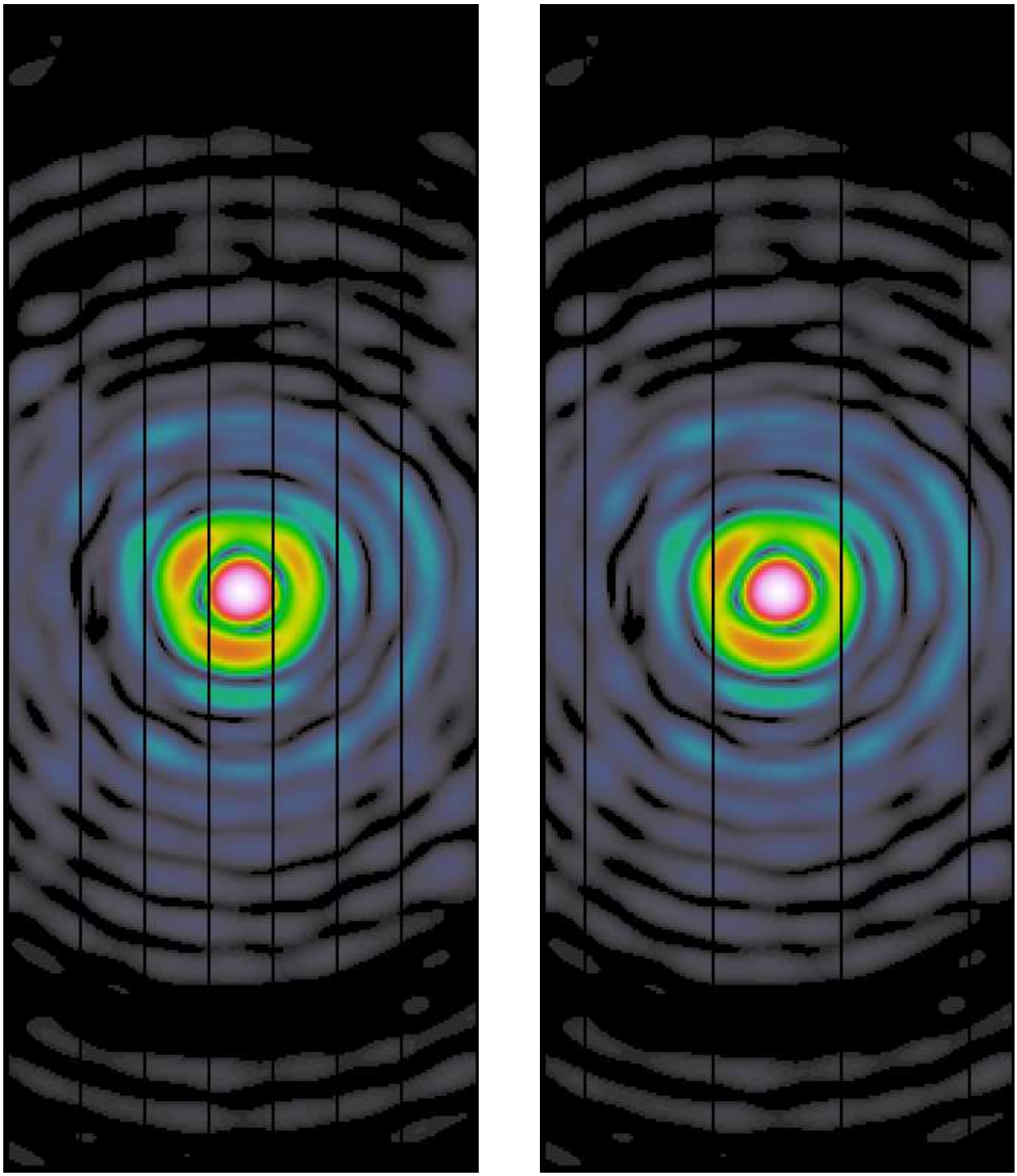

Figure 2: Model PSF subsampled to dimensions of 0.1 pixel, with overlays of the 5 slit placements of the 52x0.1 slit (left) and the 3 slit placements of the 52x0.2 slit (right). The slits have been broadened by 10% to compensate for the broadening of the PSF caused by the Lyot stop.

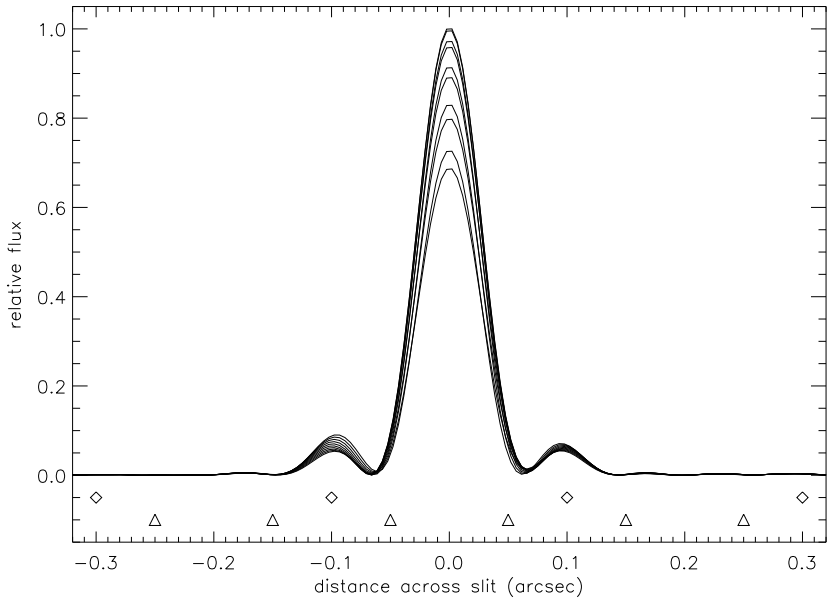

Figure 3: Profiles of the central 10 rows of the subsampled PSF (compressed by 10% in the dispersion direction to compensate for the broadening caused by the Lyot stop), with the locations of the slit edges indicated by triangles (52x0.1 slit) and diamonds (52x0.2 slit).

times pixel height for the 52x0.1 observations, and over grids of 44 by 10 subpixels to represent (broadened) slitwidth times pixel height for the 52x0.2 observations. The target was assumed to be centered in the central slit in the x (dispersion) direction, since the ACQ/PEAKs performed with the 52x0.1 slit achieved this centering with an accuracy of a tenth of a pixel. Since there is no constraint on the y positioning of the spectrum within a pixel at a given column, the summation was performed 10 times, stepped by one subpixel in the y dimension each time, to give 10 sets of PSFs to compare to the data. PSF sets separated by 5 subpixel steps in y thus correspond to the half-pixel dither pairs in the data.

Before comparison of the PSFs to the data, one additional procedure was necessary: the simulation of charge diffusion on the CCD. An electron not strongly held within the pixel where it was liberated by a photon can wander into an adjacent pixel. (See Krist 2003 for a detailed discussion.) Therefore, for each slit position and y-centering, the single column of numbers representing the PSF along the slit was convolved with a one dimensional charge diffusion kernel. The input file generated by Tiny Tim gives symmetric 3 pixel by 3 pixel kernels at different wavelengths, so that a kernel can be computed for a particular wavelength by interpolation. (Tiny Tim automatically uses these kernels to apply charge diffusion to the PSF unless it is sampled at the subpixel level.) For the spectroscopic modelling, the 3x3 6600 Å kernel was collapsed to the y dimension. This reflects the fact that the structure of the PSF in the x dimension is lost in a spectral image. Convolution of a locally flat spectrum in a spectral image by this 1x3 kernel and by the original 3x3 kernel are equivalent.

Figure 4 shows the spectroscopic PSF for the target-centered 52x0.1 slit before blocking the subpixels into pixels (dot-dashed line), after the blocking (dashed line), and after applying charge diffusion (solid line). The blocked charge-diffused profile can be interpreted as a PSF generated by taking finely spaced along-the-slit dither steps with the CCD. For a single exposure, one must choose points on that profile at intervals of 0.05 arcsec (one CCD pixel).

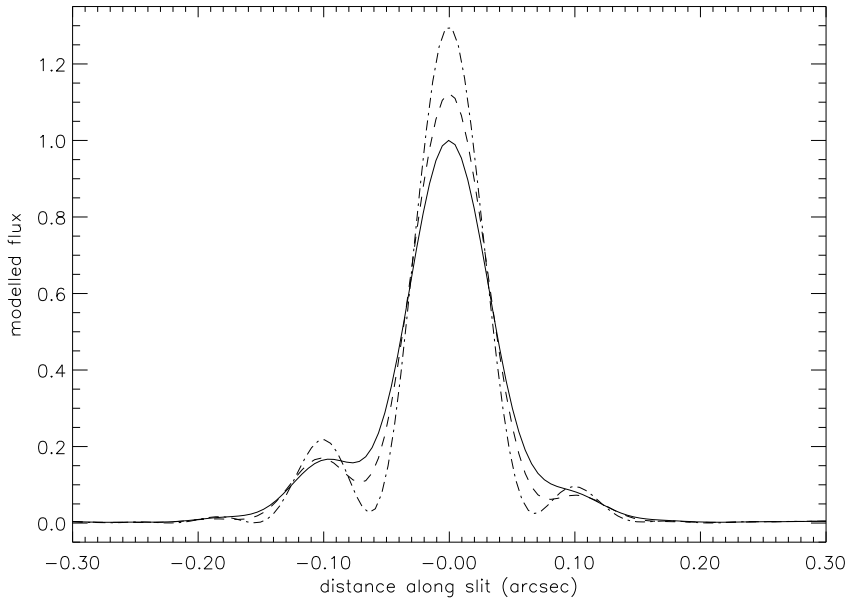

Figure 4: The spectroscopic PSF for the target-centered 52x0.1 slit before blocking the subpixels into pixels (dot-dashed line), after the blocking (dashed line), and after applying charge diffusion (solid line).

The spectroscopic PSF modelling technique treats the aperture as a mask placed on the PSF. For a spectroscopic exposure of a star centered in the 0.2x0.2 aperture, the modelled flux in the cross-dispersion direction would be limited to 4 or 5 pixels before applying charge diffusion (depending on how the aperture is centered on the rows of pixels), and would be spread to a total length of 6 or 7 pixels by the charge diffusion kernel. In practice, the flux trails off to a greater distance, due to unaccounted for diffracted and scattered light. Figure 5 shows the 6600 Å spatial profiles of the flux of the star HD101998 observed through the 0.2x0.2 and 52x0.2 apertures (exposures o4sp04030 and o4sp04040, made consecutively within a timespan of eight minutes in program 7932). The profiles have been normalized by a constant to facilitate comparison of fluxes to the peak flux. The plot on the right is scaled to better show the pixels beyond the central 7 rows, where the model would indicate flux=0 for the 0.2x0.2 aperture profile. The observed excess flux in the 0.2x0.2 aperture profile in this region, neglected by the model, is a substantial fraction of the flux observed in the 52x0.2 profile.

Comparison Of Data And Models

The flux profile along the central slit in each observing pattern was compared to the modelled profiles. The modelled profiles with the y-centering that best matched the data were selected. The modelled profiles were normalized so that the greatest value achieved in any of the ten sets of y-steps was 1.0. The data were scaled to match the modelled profiles by requiring the flux summed over the central 0.25 arcsec in the central slit to match the sum of the PSF values over that region.

Figure 6 shows the observed flux along the central slit (position 3 of 1,2,3,4,5) and the PSF model prediction for the 52x0.1 slit. The left column of plots shows the results for the 52x0.1 observations (centered on the detector), and the right column shows those for the 52x0.1E1 observations (high on the detector). The three rows of plots show different ranges in intensity and distance along the slit. The models are a good match

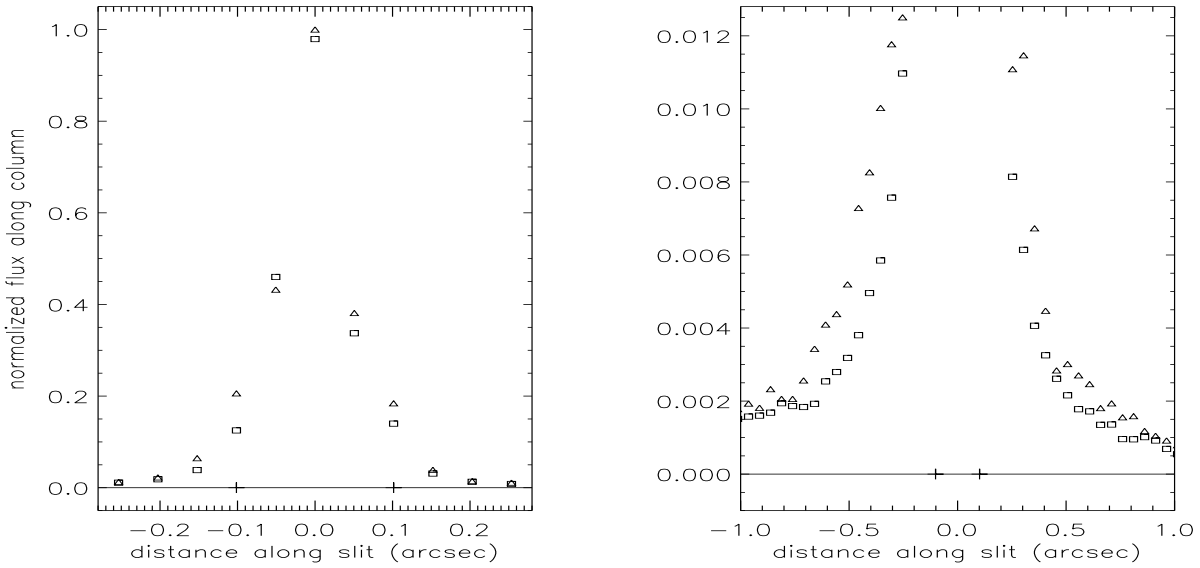

Figure 5: Observed flux along the slit for the 52x0.2 aperture (triangles) and the 0.2x0.2 aperture (squares) centered on a star. Different ranges in distance along the slit (arcsec) and in flux (normalized by the same constant) are shown in the two plots. Tick marks on the x=0 line indicate the height of the 0.2x0.2 aperture.

to the observed flux to about 0.15 arcsec from the center, to within the systematic errors indicated by the differences in the fluxes taken at equivalent dither positions. The fluxes are greater than predicted in the faint wings of the PSF. This is due to the halo of scattered light not included in the Tiny Tim modelling, as discussed above.

Figure 7 shows the central slit flux profile for 52x0.1 again, modelled and observed, in the central panel. The adjacent panels show the flux profiles for the intermediate and outer slit positions in the 5-step observing pattern. The modelled profiles in the intermediate and outer positions do not match the shape of the observed profiles, and generally over-predict the flux. This is unexpected, since defocus or excess jitter in tracking would generally cause more flux than predicted to appear in the offset apertures.

Figure 8 gives a comparison of the observed flux profiles for the 52x0.1 and the 52x0.1E1 pattern positions. The differences between the apertures are generally comparable to the systematic differences between the dither steps, indicating that the spectroscopic PSF is not significantly position dependent.

Figure 9 shows the PSF model prediction and the observed flux along the central slit (position 2 of 1,2,3) for the 52x0.2 slit. Analogous to Figure 6, the left column of plots shows the results for the 52x0.2 observations (centered on the detector), and the right column shows those for the 52x0.2E1 observations (high on the detector). The three rows of plots show different ranges in intensity and distance along the slit. As was the case for the narrower slit, the models are a good match to the observed flux to about 0.15 arcsec from the center. The fluxes are greater than predicted in the faint wings of the PSF, again due to the scattered light halo.

Figure 10 shows the central slit profile for 52x0.2 again, modelled and observed, in the central panel. The adjacent panels show the profiles for the outer slit positions in the 3-step observing pattern. The modelled profiles in the outer positions over-predict the flux by a factor of about 5 at the peak. The model predictions are sensitive to the position and structure of the first Airy ring, as can be seen in Figures 2 and 3.

Figure 11 gives a comparison of the observed flux profiles for the 52x0.2 and the 52x0.2E1 pattern

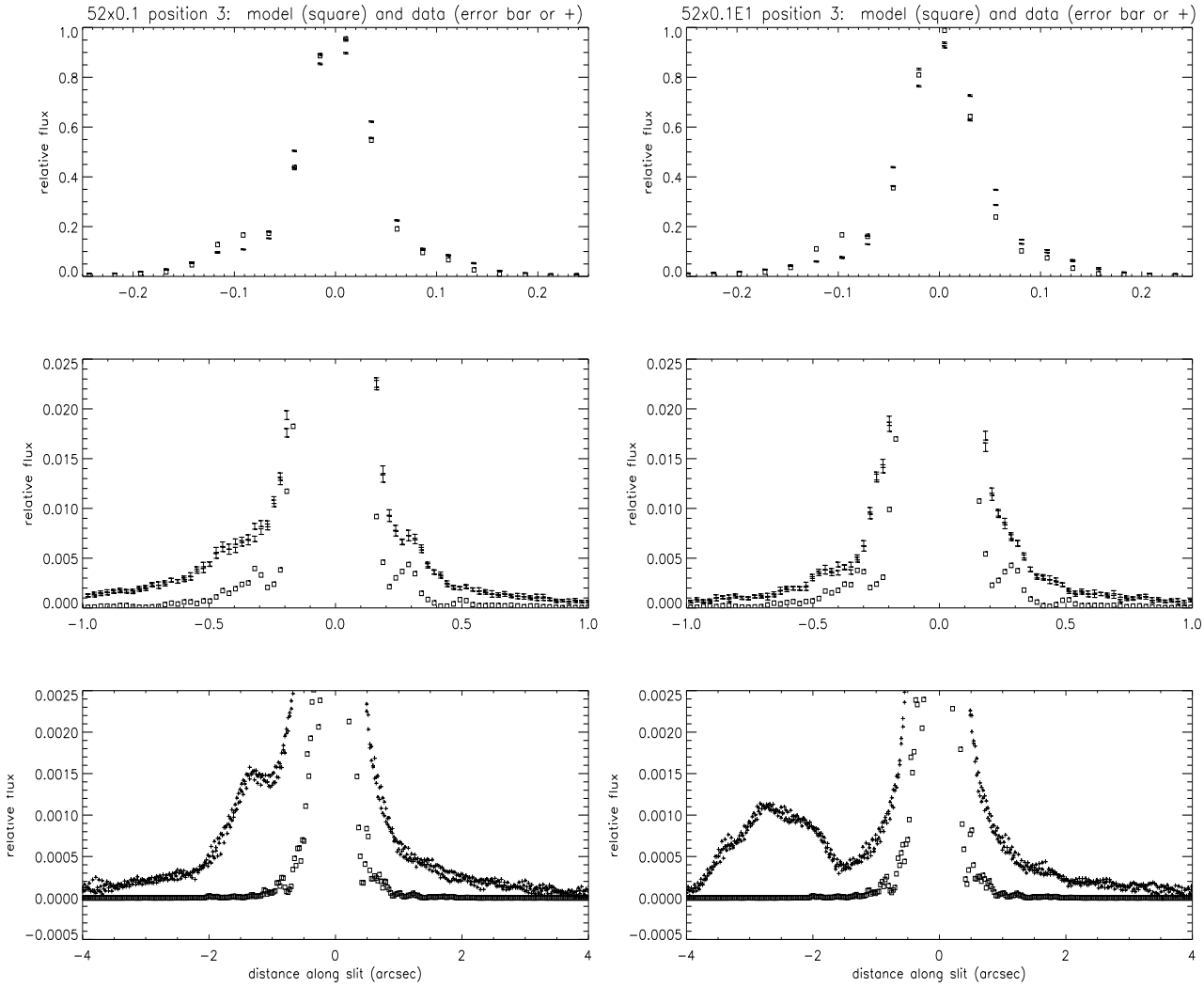

Figure 6: Observed flux along the slit (error bars or +) and PSF model prediction (squares) for the 52x0.1 aperture (left) and the 52x0.1E1 aperture (right) centered on the star. Three ranges in distance along the slit (arcsec) and in flux (normalized as described in the text) are shown.

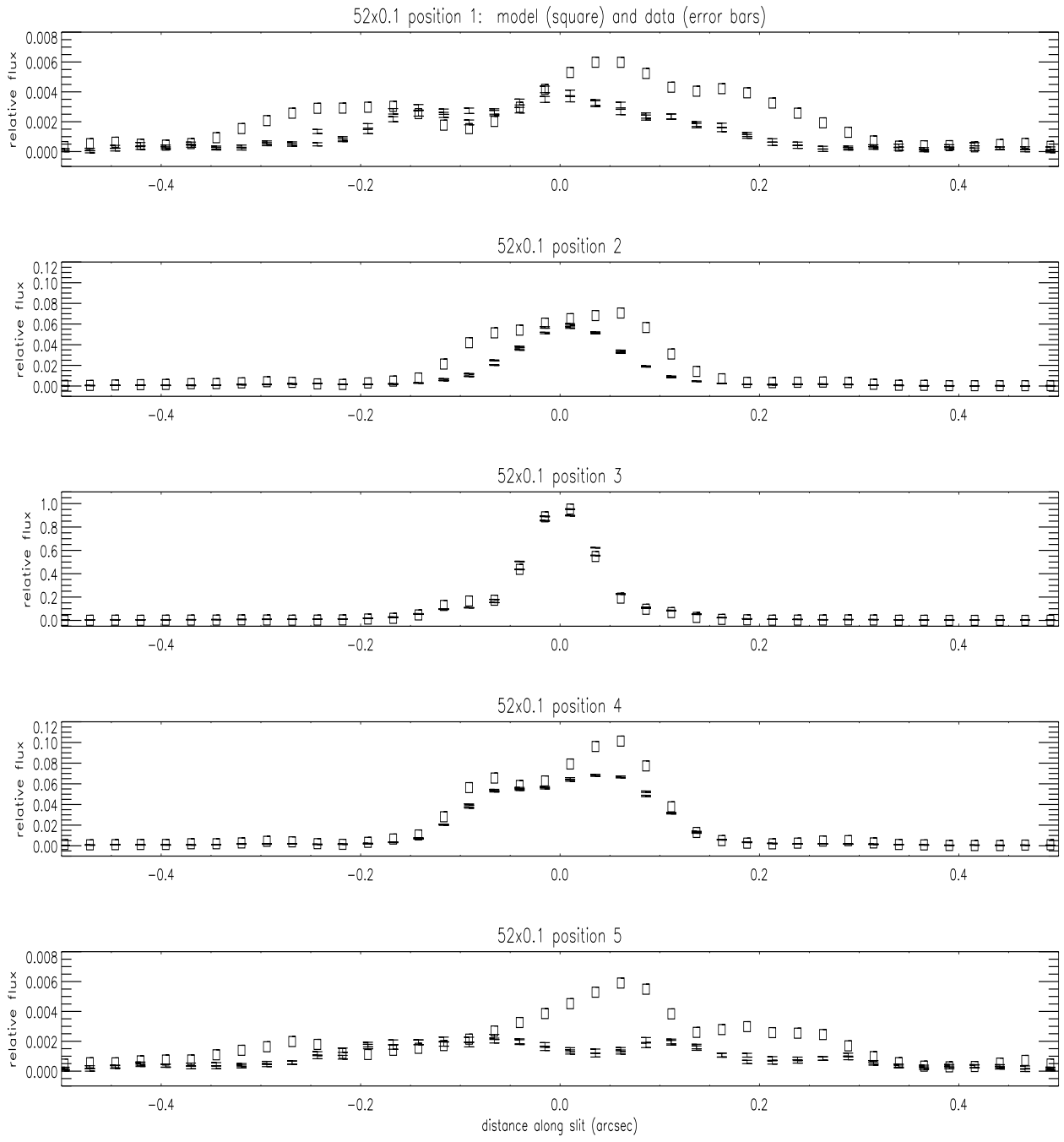

Figure 7: Observed profiles (error bars) and modelled profiles (squares) of flux along the slit for each of the 5 placements of the 52x0.1 aperture. Flux is relative to the greatest model flux for the target-centered placement (position 3).

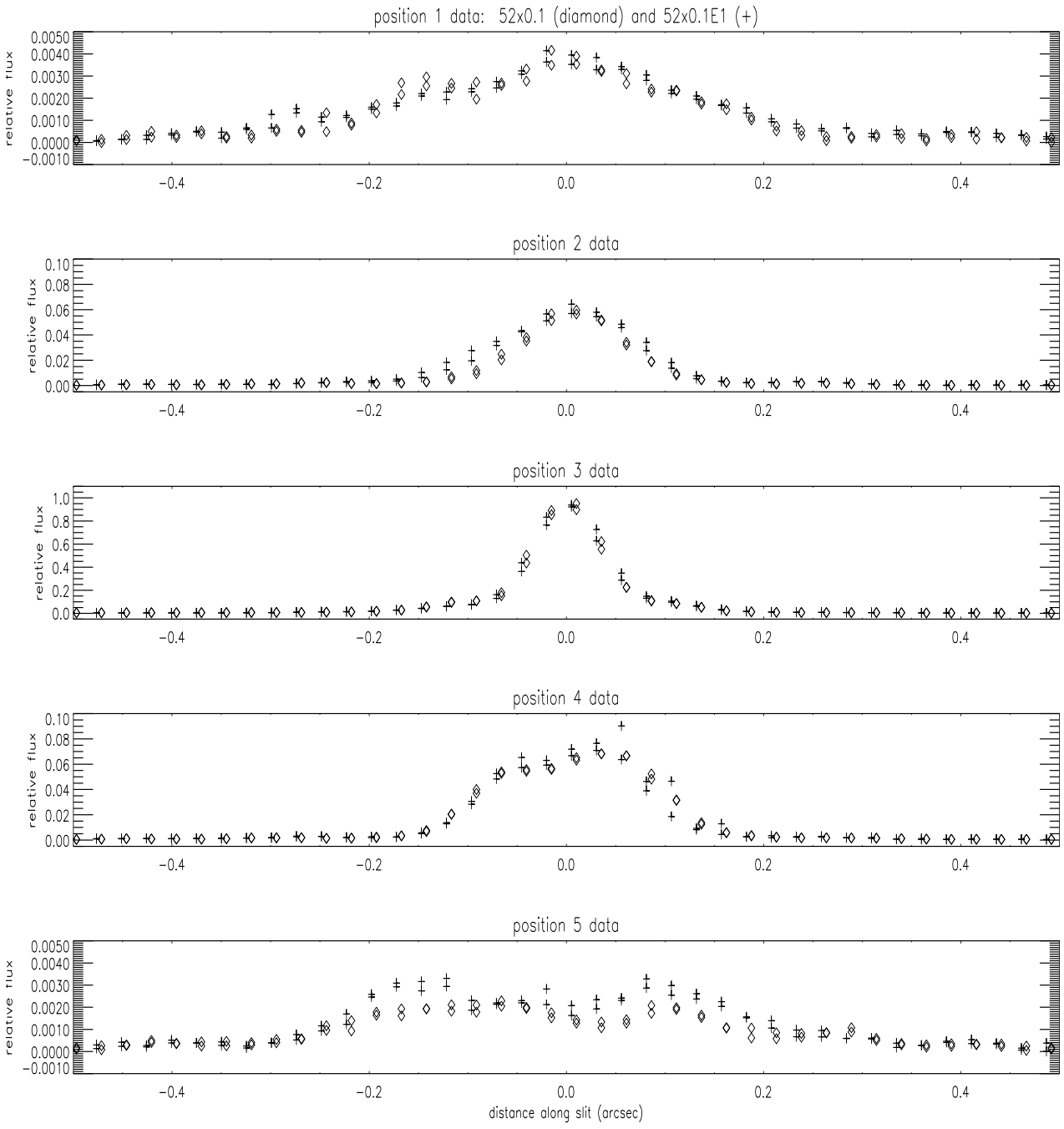

Figure 8: Observed profiles of flux along the slit for each of the 5 placements of the 52x0.1 aperture (diamonds) and the 52x0.1E1 aperture (+). Flux is relative to the greatest model flux for the target-centered placement (position 3).

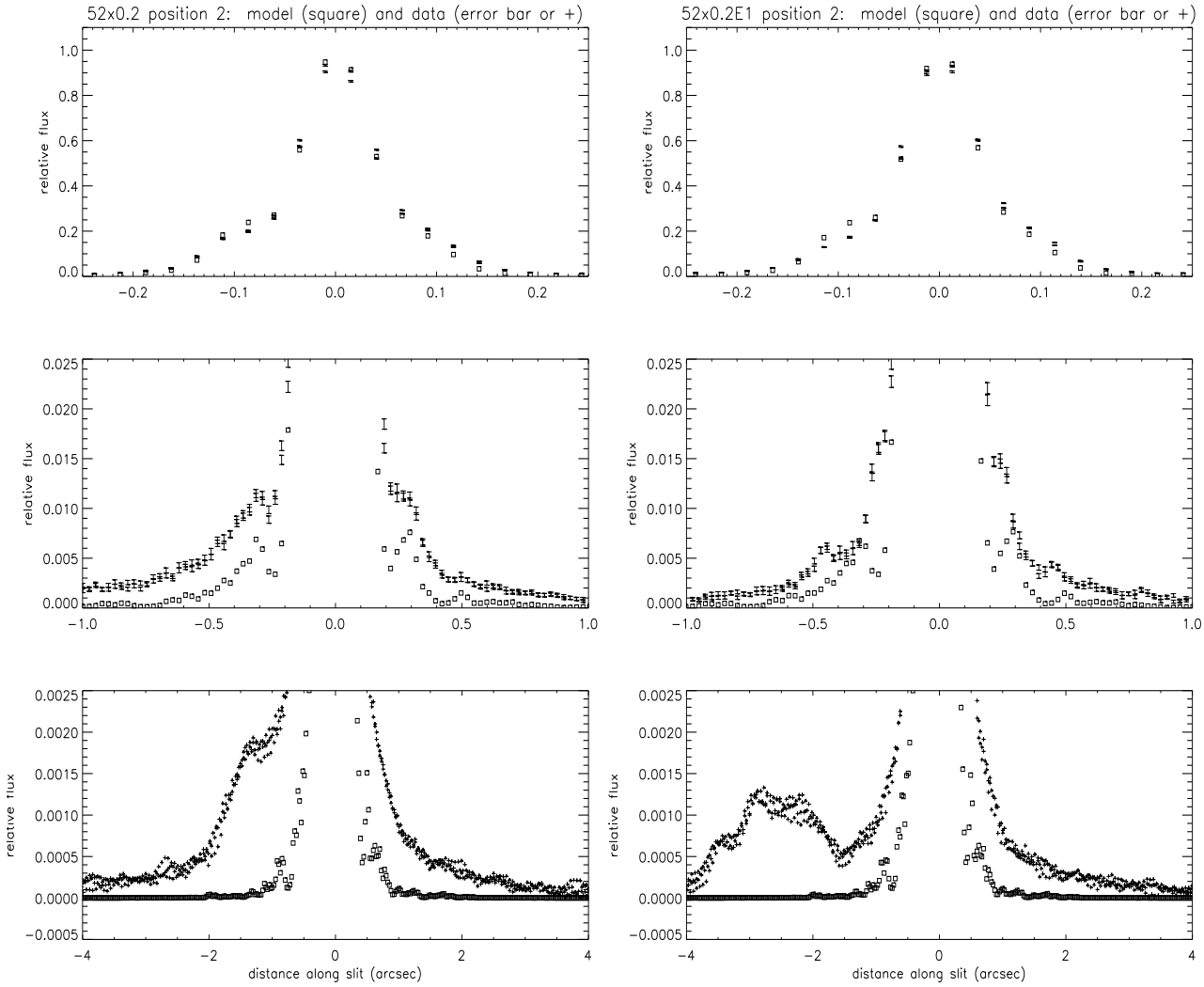

Figure 9: Observed flux along the slit (error bars or +) and PSF model prediction (squares) for the 52x0.2 aperture (left) and the 52x0.2E1 aperture (right) centered on the star. Three ranges in distance along the slit (arcsec) and in flux (normalized as described in the text) are shown.

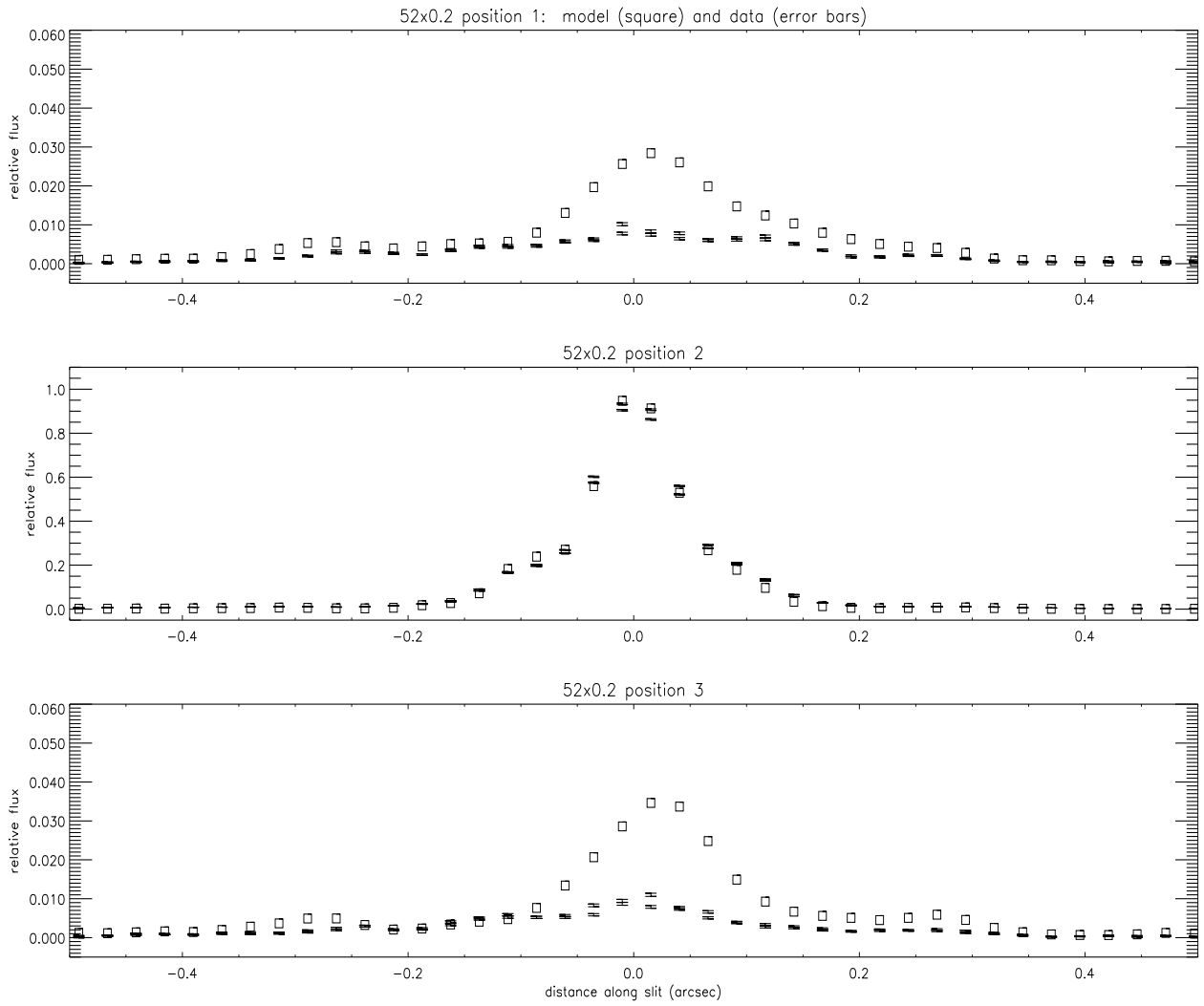

Figure 10: Observed profiles (error bars) and modelled profiles (squares) of flux along the slit for each of the 3 placements of the 52x0.2 aperture. Flux is relative to the greatest model flux for the target-centered placement (position 2).

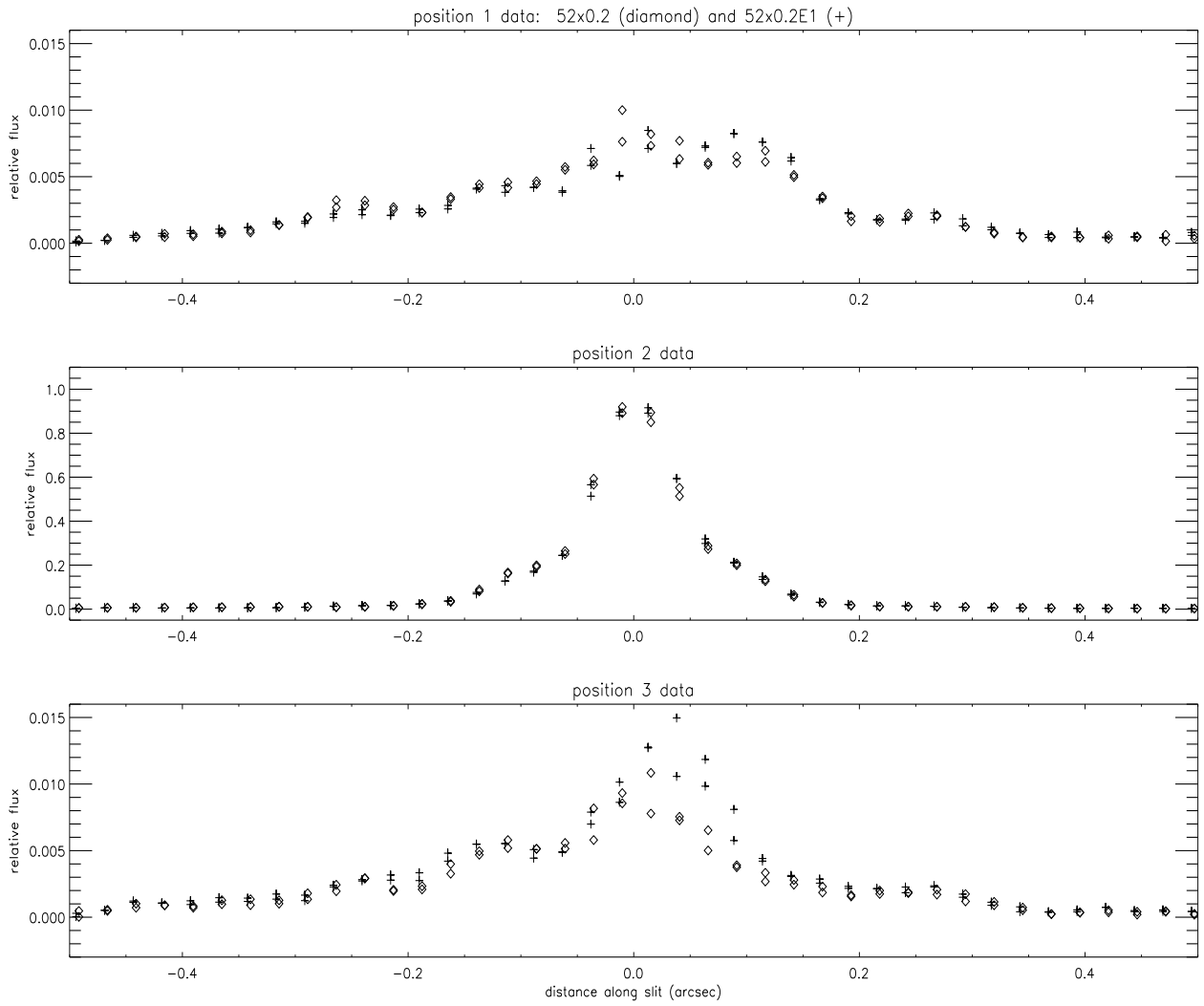

Figure 11: Observed profiles of flux along the slit for each of the 3 placements of the 52x0.2 aperture (diamonds) and the 52x0.2E1 aperture (+). Flux is relative to the greatest model flux for the target-centered placement (position 2).

positions. As for the narrower slit, the differences are fairly modest, except where the systematic errors in the data are large.

To examine the symmetry of the observed flux distributions, the flux along the column in each observing position was summed over a length equal to the slitwidth, combining the dither steps. The summed fluxes can then be displayed in a 5x5 pattern of 0.1"x0.1" blocks for the 52x0.1 aperture, and in a 3x3 pattern of 0.2"x0.2" blocks for the 52x0.2 aperture. The Tiny Tim model fluxes were handled in a similar way, combining fluxes from the PSFs corresponding to the dither steps and blocking them over the appropriate dimensions, modifying the slit width to take into account the narrower PSF prior to the Lyot stop. The results are shown in Tables 1 and 2 for the 52x0.1 and 52x0.2 apertures, respectively, with the slits displayed in the order that they would be placed left to right on a STIS image of the star. The fluxes in each block have been normalized by the flux in the central block. The tables show the observed fluxes, the modelled fluxes, and the ratio of modelled to observed flux.

Table 1: Fluxes summed over blocks of slitwidth*slitwidth for aperture 52x0.1: observed (top), model (center), ratio of model to observed (bottom)

x	$slit5$	$slit4$	$slit3$	$slit2$	$slit1$
+0.2"	0.0012	0.0047	0.0186	0.0025	0.0013
+0.1"	0.0024	0.0566	0.1652	0.0229	0.0033
0.0"	0.0022	0.0853	1.0000	0.0701	0.0048
−0.1"	0.0028	0.0418	0.1492	0.0147	0.0036
−0.2"	0.0020	0.0030	0.0245	0.0027	0.0020
+0.2"	0.0039	0.0043	0.0067	0.0062	0.0049
+0.1"	0.0063	0.0812	0.1343	0.0611	0.0069
0.0"	0.0060	0.1050	1.0000	0.0879	0.0065
−0.1"	0.0029	0.0568	0.1820	0.0434	0.0028
−0.2"	0.0019	0.0048	0.0128	0.0041	0.0042
+0.2"	3.21	0.92	0.36	2.49	3.80
+0.1"	2.63	1.43	0.81	2.67	2.10
0.0"	2.72	1.23	1.00	1.25	1.36
−0.1"	1.02	1.36	1.22	2.95	0.77
−0.2"	0.97	1.59	0.52	1.50	2.09

Table 2: Fluxes summed over blocks of slitwidth*slitwidth for aperture 52x0.2: observed (top), model (center), ratio of model to observed (bottom)

x	$slit3$	$slit2$	$slit1$
+0.2"	0.0043	0.0753	0.0068
0.0"	0.0148	1.0000	0.0140
−0.2"	0.0067	0.0927	0.0069
+0.2"	0.0120	0.0445	0.0136
0.0"	0.0457	1.0000	0.0398
−0.2"	0.0076	0.0819	0.0101
+0.2"	2.78	0.59	2.01
0.0"	3.09	1.00	2.84
−0.2"	1.14	0.88	1.47

The modelled flux distributions are somewhat asymmetric, with flux dropping off from the peak faster in a step perpendicular to the slit than in a comparable step along the slit. Some asymmetry is to be expected because of the azimuthal structure in the Airy rings, and because of the effectively one dimensional nature of the charge diffusion. Using Tables 1 and 2, the asymmetry can be quantified by taking the ratio of the blocked fluxes adjacent to the central block in the spatial direction to the blocked fluxes adjacent to the central block in the dispersion direction. The asymmetry ratios of the spectroscopic Tiny Tim models are thus (0.182+0.134)/(0.105+0.088) = 1.6 for the 52x0.1 aperture and (0.082+0.045)/(0.046+0.040) = 1.5 for the 52x0.2 aperture. Before charge diffusion is applied, the asymmetry ratio is 1.4 for both apertures, indicating that the asymmetry in the models is dominated by the structure in the Airy rings. As expected from Figures 7 and 10, the observed flux distributions are much more asymmetric than the modelled ones, with even lower fluxes in the offset slits. The observed asymmetry ratios are 2.0 for the 52x0.1 aperture and 5.8 for the 52x0.2 aperture.

As seen in Figure 2, the first Airy dominates the flux in the 52x0.1 slit at offsets of one slitwidth. In this figure and in the flux modelling, the slit has been broadened by 10% to compensate for the 10% broadening of the PSF downstream by the Lyot stop. A minor error in the broadening factor would not appreciably change the contribution of the Airy ring to the offset slits. A broadening of 30% would be required to make the modelled asymmetry factor match the observed one for this slit. The HST PSF at the slit cannot be as narrow as that would imply, so uncertainty in the broadening of the PSF by the Lyot stop cannot account for the discrepancies between the observed and modelled fluxes.

For the STIS CCD detector, Tiny Tim parameters were derived for images taken with a clear aperture, a broadband filter, and two narrowband filters. Images made with the narrowband filters, F28X50OII at 3737 Å and F28X50OIII at 5006 Å, provide a good check of the model at those wavelengths. For 3x3 pixel blocking (0.15"x0.15"), the F28X50OIII Tiny Tim PSF and the image of a star well-centered on a pixel (exposure o3zf02010 of Feige 34), both have asymmetry ratios of 0.94. The model is less well constrained at longer wavelengths, since wavelength-dependent PSFs weighted by the source spectrum are blended together in broadband images. An alternative approach was therefore used to check the consistency of imaging PSFs and spectroscopic PSFs. Several columns in the G750L spectroscopic images were used to examine the wavelength dependence of the x-y asymmetry, to see if the spectroscopic PSF asymmetry diminished toward shorter wavelengths, approaching the symmetry found for imaging at 5006 Å. This was not the case. Similar degrees of asymmetry were found for the observed spectroscopic PSF from 5500 to 7750 Å, greater in all cases than the asymmetry of the modelled spectroscopic PSF. The observed and modelled asymmetry ratios are given for a series of wavelengths in Table 3. If there were a change in the astigmatism of the PSF longward of 5000 Å, it would have to be rather abrupt, and would have to be similar at two widely separated positions on the detector, given the similarity of the spectroscopic profiles at 6600 Å for the regular and E1 apertures.

Table 3: X-Y asymmetry ratios of the spectroscopic PSF as a function of wavelength

CCD column	*wavelength* (Å)	52x0.1 *data*	52x0.1 *model*	52x0.2 *data*	52x0.2 *model*
50	5490	2.4	1.5	4.5	1.8
170	6070	2.1	1.6	5.8	1.7
277	6600	2.0	1.6	5.8	1.5
450	7440	2.1	1.5	4.8	1.3
512	7745	2.1	1.5	4.3	1.2

An assumption of the modelling is that the summation of the observed fluxes in the five contiguous

positionings of the 52x0.1 slit should equal the flux observed in the 52x0.5 slit. The summation of the observed fluxes in the three contiguous positionings of the 52x0.2 slit should be similar to the flux in the 52x0.5 slit, since the flux at the outer edges of the 52x0.5 slit is small. The 52x0.5 slit was not used in program 9610, but the same star was observed with the 52x0.5E1 aperture in program 8929 one year earlier. The profiles of the 6600 Å flux along the slit are shown in Figure 12 for the summed 52x0.1E1 observations, the summed 52x0.2E1 observations, and the single 52x0.5E1 observation. Fluxes from dither positions separated by half a pixel along the slit are shown for the summed observations; the 52x0.5E1 observation was not dithered. The summed 52x0.2E1 fluxes nearly equal the 52x0.5E1 fluxes, but the summed 52x0.1E1 fluxes are noticeably lower. Using the dither positions that most closely match the 52x0.5E1 observation and summing the fluxes over 7 pixels (0.35 arcsec) along the slit, the summed 52x0.1E1 flux and summed 52x0.2E1 flux are 83% and 98.5% of the 52x0.5E1 flux, respectively. The errors in each 7-pixel flux are 0.5% or less, as determined by the actual differences in the fluxes produced by dithering (i.e., not just the statistical errors). There is no 52x0.5 aperture observation of this star at the center of the detector, but the summed 52x0.1 aperture flux is lower than the summed 52x0.2 aperture flux (88% as much flux over 0.35 arcsec along the slit), similar to the result for the E1 apertures. The profiles for the summed 52x0.1 fluxes and the summed 52x0.2 fluxes are shown in Figure 13. The reason for this repeatable discrepancy is not apparent. As discussed earlier, the changes in focus due to breathing were insignificant during these observations, and pointing errors were small. The slit sizes have been well measured (Bohlin and Hartig 1998) and the stepping patterns should have provided very nearly contiguous placements of the slits. Temperature-dependent and time-dependent sensitivity changes for this grating and time span are negligible (Stys et al. 2004). A remaining possibility is that the empirical treatment of the effect of the Lyot stop on the slitted PSF may be inadequate.

Comparison of G750M to G750L

The G750M mode, unlike the G750L mode, does not include a Lyot stop in its optical path, and therefore has a narrower PSF at the detector. Data from other HST programs have been used to make a detailed comparison of the PSFs at 6600 Å in these modes. For G750M, a single spectral image is sufficient to produce a finely sampled PSF because the spectral trace drops by 7 rows as it crosses the detector. The fractional pixel drops in the trace from one column to the next in an flt or crj image can be treated as a series of microdithers. The observed PSF is produced by normalizing out the stellar spectrum and centering the flux profile in each column on the trace. A band of many columns can be used to sample the PSF because it does not measurably change across this short span of wavelengths. A well exposed image of the calibration standard star BD+75D325 (o4a505050 from program 7656) taken with the 52X2 aperture was used to produce the G750M PSF.

The same technique cannot be used for G750L because the trace is nearly flat across the detector, producing insufficient "microdithering" of the columns in one image. In this case, the slight randomness in the placement of the spectrum on the detector (within a few rows) can be treated as a dither for a sample of many exposures. The flux profile from a single column in each image, centered according to its placement on the detector, can be used to measure the PSF at a given wavelength. Well-exposed images of the star AGK+81D266 from the STIS sensitivity monitor programs (7672, 8418, 8856, 8914, 9627, 10030) were used to produce the 52X2 G750L PSF.

A comparison of the observed 52X2 6600 Å PSFs for G750M and G750L is shown in Figure 14. The profiles expected from Tiny Tim modelling are also shown. The model for G750M is based on an imaging PSF for which the Lyot stop was effectively removed by setting its radius to a large value in the Tiny Tim input file. The 52X2 slit includes virtually all of the incident PSF, so adjustment of the slitwidth to compensate for PSF-broadening by the Lyot stop is inconsequential for the G750L modelling in this case, and no information

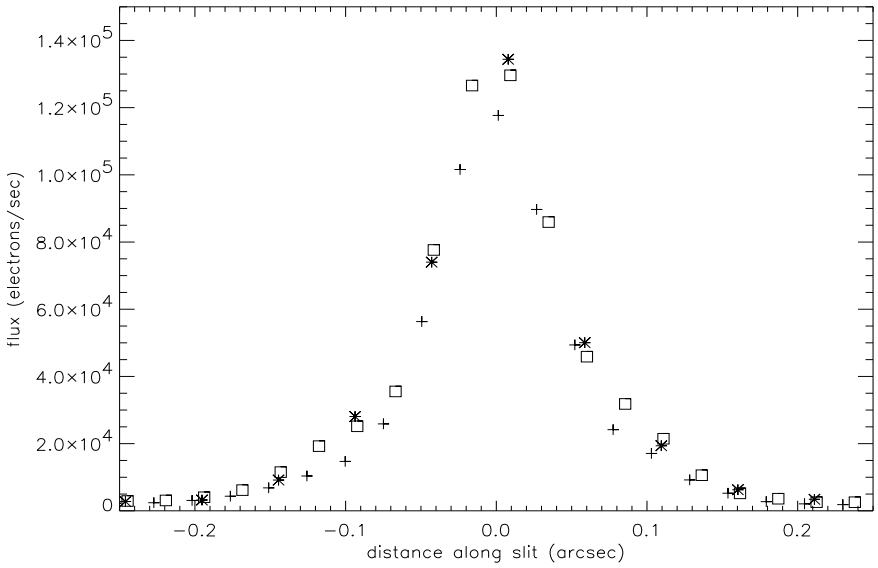

Figure 12: Observed spectroscopic PSFs: summation of fluxes in 5 contiguous positionings of aperture 52x0.1E1 (+), summation of fluxes in 3 contiguous positionings of aperture 52x0.2E1 (square), and flux in a single position of aperture 52x0.5E1 (*). Fluxes are in electrons/sec; distance along the slit is in arcsec, adjusted to center each profile at 0.

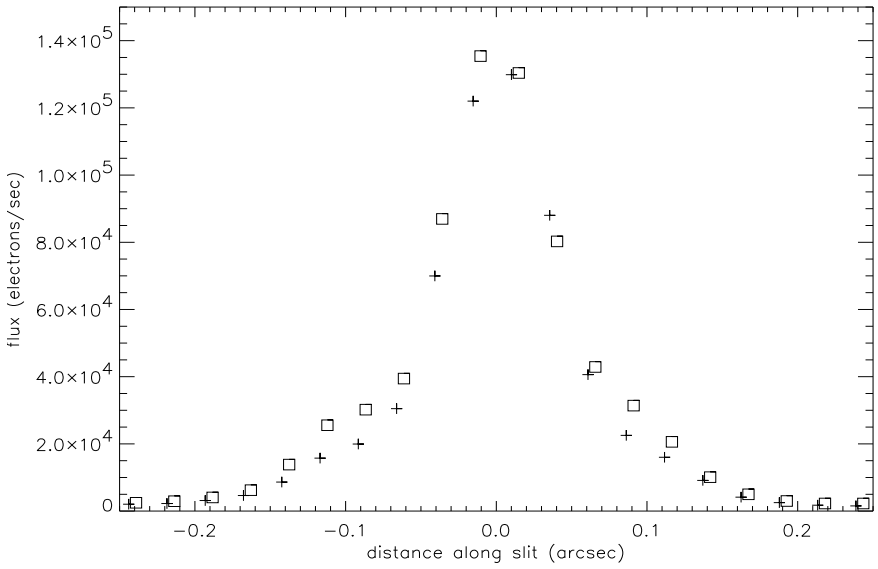

Figure 13: Observed spectroscopic PSFs: summation of fluxes in 5 contiguous positionings of aperture 52x0.1 (+) and summation of fluxes in 3 contiguous positionings of aperture 52x0.2 (square) with the target at the center of the detector. Fluxes are in electrons/sec; distance along the slit is in arcsec, adjusted to center each profile at 0.

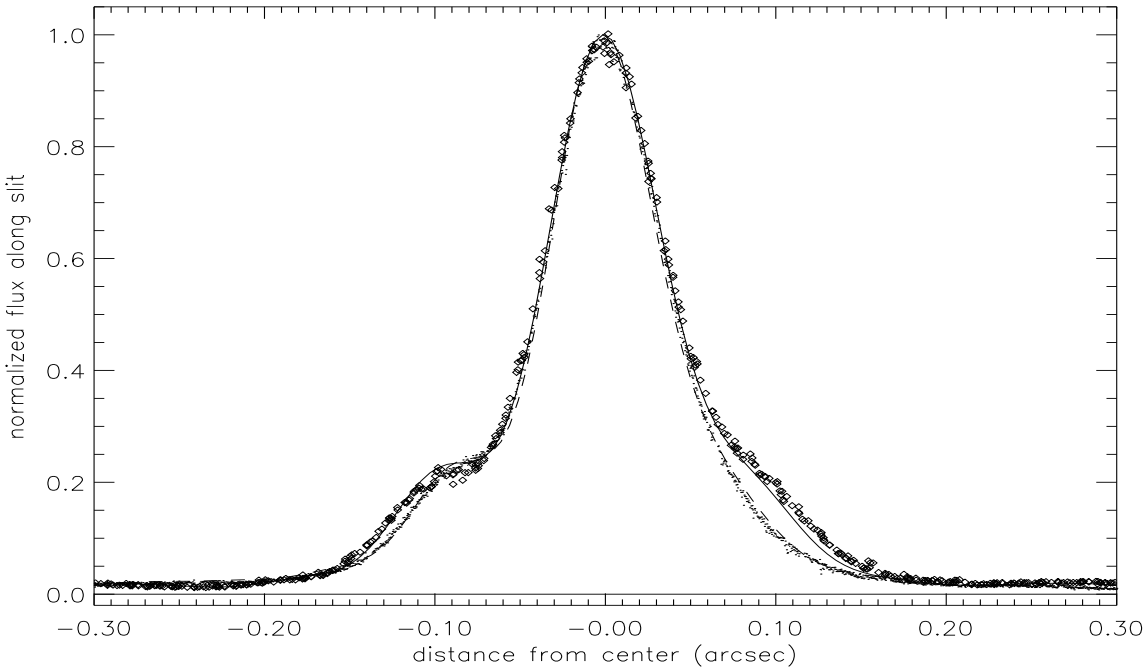

Figure 14: 6600 Å PSFs for 52X2 G750L (data: diamonds, model: solid line) and G750M (data: dots, model: dashed line).

is gained from the data on the structure of the spectroscopic PSF in the dispersion direction. The effect of the Lyot stop on the PSF in the cross-dispersion direction is clearly seen in the data, and the modelling shows good consistency with the data for both gratings. The most conspicuous difference between the G750L and G750M profiles is the broader ”shoulders” of the G750L PSF. The coarse sampling by pixels and the charge diffusion on the detector can obscure the source of the difference, as seen in Figure 4. Figure 1 indicates that the source of the difference in the modelling is an overall expansion of the PSF by the Lyot stop, rather than an increase of the flux in the first Airy ring relative to the flux in the Airy disk. In any case, row-to-row contamination of spectral features is somewhat less for G750M, and contamination of offset apertures by a bright out-of-slit source is also expected to be less.

Conclusions

I have compared Tiny Tim model predictions and G750L flux profiles at 6600 Å for a star centered in a slit (52x0.1, 52x0.1E1, 52x0.2, or 52x0.2E1) and moved out of the slit by one or two slit widths. The model under-predicts the flux in the centered slit at distances greater than 0.2 arcsec from the target, where it does not fully account for scattered and diffracted light. It over-predicts the flux in the offset positions, even after an empirical adjustment of the slit width to compensate for the broadening of the PSF by the Lyot stop. The observed spatial distribution of monochromatic flux generated by the stepping patterns is asymmetric, more so than expected from the azimuthal structure in the Airy rings in the Tiny Tim model. Nearly the same degree of asymmetry is observed from 5500 to 7750 Å. This asymmetry is not observed in direct narrow-band imaging at 5006 Å, which is also affected by a Lyot stop; this implicates the role of the slit in producing the asymmetry. A

discrepancy between the summation of fluxes in a narrow aperture stepped across a star and the flux in a single broad aperture centered on the star suggests that the empirical treatment of the effect of the Lyot stop on the slitted PSF may be inadequate.

The G750M grating does not have a Lyot stop, and therefore has a narrower PSF than the G750L grating at a given wavelength. The observed PSFs for these two gratings are differently shaped because of the combined effects of broadening by the Lyot stop, undersampling by pixels, and charge diffusion on the CCD. For a broad slit centered on the star, Tiny Tim modelling reproduces the observed spectroscopic PSF well for both gratings.

Acknowledgments

I would like to thank Chuck Bowers, Paul Goudfrooij, Ted Gull, George Hartig, Don Lindler, and Charles Proffitt for useful discussions and information, and Goudfrooij and Proffitt for reviewing the manuscript.

References

Bohlin, R. & Hartig, G., 1998, STIS ISR 98-20, "Clear Aperture Fractional Transmission for Point Sources".

Heap, S.R., Lindler, D.J., Lanz, T.M., Cornett, R.H., Hubeny, I., Maran, S.P., & Woodgate, B., 2000, Ap.J., 539, 435, "Space Telescope Imaging Spectrograph Coronographic Observations of Beta Pictoris".

Kim Quijano, J. et al., 2003, STIS Instrument Handbook, version 7.0 (Baltimore: STScI).

Krist, J., 2003, ACS ISR 2003-06, "ACS WFC & HRC field-dependent PSF variations due to optical and charge diffusion effects".

Stys, D.J., Bohlin, R.C., & Goudfrooij, P., 2004, STIS ISR 2004-04, "Time-Dependent Sensitivity of the CCD and MAMA First-Order Modes".